



**HAL**  
open science

**A contribution to the synsedimentary versus epigenetic origin of the Cu mineralizations hosted by terminal Neoproterozoic to Cambrian formations of the Bou Azzer–El Graara inlier: New insights from the Jbel Laassel deposit (Anti Atlas, Morocco)**

Hugo Bourque, Luc Barbanson, Stanislas Sizaret, Yannick Branquet, Claire Ramboz, A. Ennaciri, M. El Ghorfi, L. Badra

► **To cite this version:**

Hugo Bourque, Luc Barbanson, Stanislas Sizaret, Yannick Branquet, Claire Ramboz, et al.. A contribution to the synsedimentary versus epigenetic origin of the Cu mineralizations hosted by terminal Neoproterozoic to Cambrian formations of the Bou Azzer–El Graara inlier: New insights from the Jbel Laassel deposit (Anti Atlas, Morocco). *Journal of African Earth Sciences*, 2015, 107, pp.108-118. 10.1016/j.jafrearsci.2015.04.005 . insu-01145561

**HAL Id: insu-01145561**

**<https://insu.hal.science/insu-01145561>**

Submitted on 12 Jun 2015

**HAL** is a multi-disciplinary open access archive for the deposit and dissemination of scientific research documents, whether they are published or not. The documents may come from teaching and research institutions in France or abroad, or from public or private research centers.

L'archive ouverte pluridisciplinaire **HAL**, est destinée au dépôt et à la diffusion de documents scientifiques de niveau recherche, publiés ou non, émanant des établissements d'enseignement et de recherche français ou étrangers, des laboratoires publics ou privés.

## Accepted Manuscript

A contribution to the synsedimentary versus epigenic origin of the Cu mineralizations hosted by terminal Neoproterozoic to Cambrian formations of the Bou Azzer – El Graara inlier: new insights from the Jbel Laassel deposit (Anti Atlas, Morocco)

H. Bourque, L. Barbanson, S. Sizaret, Y. Branquet, C. Ramboz, A. Ennaciri, M. El Ghorfi, L. Badra

PII: S1464-343X(15)00078-3

DOI: <http://dx.doi.org/10.1016/j.jafrearsci.2015.04.005>

Reference: AES 2252

To appear in: *African Earth Sciences*

Received Date: 6 October 2014

Revised Date: 3 April 2015

Accepted Date: 4 April 2015

Please cite this article as: Bourque, H., Barbanson, L., Sizaret, S., Branquet, Y., Ramboz, C., Ennaciri, A., El Ghorfi, M., Badra, L., A contribution to the synsedimentary versus epigenic origin of the Cu mineralizations hosted by terminal Neoproterozoic to Cambrian formations of the Bou Azzer – El Graara inlier: new insights from the Jbel Laassel deposit (Anti Atlas, Morocco), *African Earth Sciences* (2015), doi: <http://dx.doi.org/10.1016/j.jafrearsci.2015.04.005>

This is a PDF file of an unedited manuscript that has been accepted for publication. As a service to our customers we are providing this early version of the manuscript. The manuscript will undergo copyediting, typesetting, and review of the resulting proof before it is published in its final form. Please note that during the production process errors may be discovered which could affect the content, and all legal disclaimers that apply to the journal pertain.



1        **A contribution to the synsedimentary versus epigenic origin of the Cu**  
2        **mineralizations hosted by terminal Neoproterozoic to Cambrian formations**  
3        **of the Bou Azzer – El Graara inlier: new insights from the Jbel Laassel**  
4        **deposit (Anti Atlas, Morocco).**

5        H. Bourque <sup>(1)\*</sup>, L. Barbanson <sup>(1)</sup>, S. Sizaret <sup>(1)</sup>, Y. Branquet <sup>(1)</sup>, C. Ramboz <sup>(1)</sup>, A. Ennaciri <sup>(2)</sup>, M. El  
6        Ghorfi <sup>(3)</sup> and L. Badra <sup>(4)</sup>

7        <sup>(1)</sup>*Institut des Sciences de la Terre d'Orléans (ISTO), UMR 7327-CNRS/Université d'Orléans/BRGM, Orléans,*  
8        *France*

9        <sup>(2)</sup>*Managem Group, Casablanca, Morocco*

10       <sup>(3)</sup>*Faculté des Sciences et Techniques – Guéliz, Bd. Abdelkrim El Khattabi - B.P. 549– Marrakech, Morocco*

11       <sup>(4)</sup>*Université Moulay Ismail, Meknès, Morocco*

12       \* Correspondence to:

13       [hugo.bourque@cnrs-orleans.fr](mailto:hugo.bourque@cnrs-orleans.fr)

14       Institut des Sciences de la Terre d'Orléans

15       UMR 7327-CNRS/Université d'Orléans

16       1A rue de la Ferrollerie

17       45071 Orléans Cedex 2

18       France

19       T : +33 (0)2 38 49 27 64

20

21

22 **Abstract**

23 The Neoproterozoic to Cambrian formations that compose the cover of the Bou Azzer-El  
24 Graara inlier, host a great number of Copper occurrence whose origin is largely discussed. To bring  
25 some light to this debate, structural, petrographic and geochemical observations were performed on  
26 the copper deposit of Jbel Laassel. This deposit, located at the extreme ESE of the Bou Azzer –El  
27 Graara inlier, is mined since 2012. At the district scale, the ore bodies localize in a folding band that  
28 extends along a NE-SW direction. At macroscopic, microscopic and scanning electron microscope  
29 scales the mineralization appears as banding veins, with locally cockade breccia and comb quartz  
30 textures. From the macroscopic scale to the scale of the scanning electron microscope, all these  
31 mineralized textures are connected there between forming a stockwork with an auto-similar structure  
32 in the range of used scales of observation. At the district scale, this stockwork is preferentially located  
33 in the anticlinal hinges of the folding band. Principal component analyses of geochemical database  
34 enable to distinguish several groups of chemical elements, each of these groups corresponding to the  
35 different lithologies and to the copper mineralization. This last group doesn't show any correlation  
36 with the distinguished lithological groups. All these observations bring new arguments to an  
37 epigenetic origin for the copper mineralization of the Jbel Laassel deposit, with a formation  
38 contemporary or posterior with the folding band development attributed to Variscan deformation.

39

40 **Keywords:** Anti-Atlas, Cu-mineralization, folding band, stockwork, epigenetic.41 **1. Introduction**

42 More than 200 Copper mineralizations are known over a large part of the Neoproterozoic to  
43 Cambrian cover in the Anti-Atlas (fig. 1A) (Bouchta et al., 1977). They are localized at different  
44 stratigraphic levels within the cover and present different characteristics. Their origin remains in most

45 cases currently poorly understood and there is no general model for this copper mineralization. Several  
46 genetic interpretations have been proposed on specific deposits: (i) based on textural and petrological  
47 observations, Leblanc (1986) suggests that Alous mineralization crystallized during the cooling of an  
48 ignimbrite; (ii) For the Cu-occurrences of Tizert, Talat N'Ouamane, Tizirt and Amadou, Pouit  
49 (1966), Bouchta & al (1977) and Skacel (1993) consider these mineralizations generated through a  
50 synsedimentary process arguing of a strong paleogeographic control of the ores. Moreover, the Cu-  
51 mineralizations hosted in the Neoproterozoic to Cambrian cover in the Anti-Atlas can be differentiate  
52 by their morphologies as veins, dissemination or stratiform bodies, without relationship have been  
53 established between these morphologies yet (Pouit, 1966; Skacel, 1993). As the result, the syngenetic  
54 or epigenetic nature of that mineralization remains still undetermined (Pouit, 1966). New data and  
55 evidences are then necessary. The Jbel Laassel deposit is one of these numerous cover-hosted copper  
56 occurrences known in the Anti-Atlas terminal Neoproterozoic to Cambrian cover, often called  
57 Adoudounian cover (Pouit, 1966; Bouchta et al., 1977; Benssaou & Hamouni, 1999). Since the 60's,  
58 various genetic models were proposed by several geologists hired by Managem Goup for the copper  
59 mineralization at Jbel Laassel site. Maacha et al. (2011) resumed these different models: in 1964 the  
60 mineralization was attributed to a porphyry copper type, in 1967 it was interpreted as a stratiform  
61 synsedimentary deposit, with a re-concentration stage associated to a Jurassic doleritic intrusion, in  
62 1978 an epigenetic origin was proposed for this mineralization with a mainly vein-shaped texture and  
63 a close association with barite. Some authors evoked a synsedimentary genesis for the Jbel Laassel  
64 deposit, where mineralization is controlled by the basement paleogeography and were locally  
65 remobilized by a tectonic event (Pouit, 1966; Bouchta et al., 1977). According to Skacel (1993),  
66 copper should be synchronous with sedimentation; its precipitation being regulated by the redox  
67 conditions, themselves under the control on the deposition environment.

68 In 1984, the MANAGEM Group discovered the potential of the Jbel Laassel Cu-  
69 mineralizations. Different preliminary estimations were performed until 2006 (Maacha et al., 2011). In  
70 2010 Managem decided to lead a core drill campaign to estimate the feasibility of this deposit. This  
71 work resulted in an estimation of 7.5 million tons at 1% Cu (Maacha et al., 2011) and the exploitation

72 began in 2012 with SOMIFER as operator. In this article, based on MANAGEM Group pre-  
73 exploitation targeting, we report the main results of an original study performed on Jbel Laassel Cu-  
74 mineralization. This work consists of: (i) a structural analysis of ore bodies, (ii) a mineralogical study  
75 of samples collected both on outcrops and drill cores and (iii) a statistical analysis of the first chemical  
76 analyses carried out in this deposit. These new data bring out new insights on the debated, epigenic  
77 versus syngenetic origin of the Jbel Laassel deposit.

## 78 **2. Geological setting**

### 79 **2.1. The Bou Azzer El Graara inlier**

80 The Bou Azzer El Graara inlier is one of a series of Proterozoic windows oriented NW-SE that  
81 expose Panafrican formations in the central part of the Anti-Atlas (Choubert, 1947). The Proterozoic  
82 basement is mainly composed by a dismembered ophiolitic sequence and arc fragments (Leblanc,  
83 1975; Saquaque et al., 1989) (fig. 1B). These formations are unconformably overlain by a thick  
84 Neoproterozoic to Cambrian volcano-sedimentary cover (Soulaimani et al., 2014). This cover can be  
85 divided into three formations from bottom to top: (1) The Tiddiline Formation (~750 to 650 Ma)  
86 attributed to the “Saghro Group” (Thomas et al. 2004), composed of clastic, volcanoclastic and  
87 volcanic series, rests mainly unconformably on the Panafrican substratum; (2) The Ouarzazate Group  
88 (~610 to 550 Ma), composed of a volcano sedimentary complex, rests in angular unconformity on the  
89 Tidiline Formation; (3) Terminal Neoproterozoic to Cambrian Formations consisting of detrital and  
90 carbonated series (Soulaimani et al., 2013). These Terminal Neoproterozoic to Cambrian Formations,  
91 varying in age from terminal Neoproterozoic to the middle Cambrian, are associated with a major  
92 marine transgression toward the Southeast and can be subdivide into two groups: the Taroudannt  
93 Group and the Tata Group (fig. 2). During the Late Paleozoic compressional event, the Panafrican  
94 structures of the basement were reactivated along the inlier’s borders. This results in box-shaped folds  
95 distributed throughout the Bou Azzer-El Graara area and by large open synclines of Cambrian rocks  
96 (Soulaimani & Burkhard, 2008). Upright detachment folds, from meters to decameters in scale, are

97 frequent in the lower Cambrian rocks and they exhibit a dominant NW-SE trend with subordinate NE-  
98 SW structures (Soulaimani & Burkhard, 2008).

99

## 100 **2.2. Lithostratigraphy of the Jbel Laassel Cu-deposit**

101 The Jbel Laassel deposit is hosted in the Lower Cambrian part of the Neoproterozoic to  
102 Cambrian volcano-sedimentary cover, at the extreme ESE part of the Bou Azzer-El Graara inlier, 30  
103 kilometers NE of the Bleida mine (fig. 1B). The whole of this cover is often call Adoudounian cover,  
104 it is a local appellation, and on the other hand the term Adoudou correspond to the name of a precise  
105 stratigraphic formation (Soulaimani et al, 2013). The Lower Cambrian is represented in the studied  
106 site by the Adoudou and Tikirt Formations, both belonging to the Taroudann Group, whereas the  
107 Igoudine, Amouslek, Issafene and Tazlaft Formations correspond to the Tata Group (fig. 2)  
108 (Soulaimani et al., 2013). All these formations are interlayered locally with volcanic flows dated at  
109  $534 \pm 10$  Ma (U/Pb on zircon by Ducrot & Lancelot, 1977) related to the Jbel Boho-type volcanism  
110 (Alvaro et al., 2006) (fig. 1 and 2).

### 111 **2.2.1 The Taroudannt Group**

112 The Adoudou Formation (Choubert, 1952) is represented in the area study by a basal  
113 sedimentary breccia with a thickness of 5 to 100 meter and by an alternation of dolostones and red or  
114 white clay's siltstones with a total thickness varying from 150 to 250 meters. Dolostones frequently  
115 present an intensive secondary silicification (Soulaimani et al., 2013). The Tikirt Formation (250 to  
116 300 meters thick) rests in conformity on the Adoudou Formation; it is composed essentially by  
117 sandstones frequently interlayered by centimetric clayed siltstones. The age of this formation is  
118 unknown; but the Taliwine Formation, a westward stratigraphic equivalent level has been dated by  
119 U/Pb on zircon from Early Cambrian volcanic horizons at  $521 \pm 7$  Ma and  $522 \pm 2$  Ma (Compston et  
120 al., 1992; Landing, 1998; Maloof et al., 2005). On the Jbel Laassel site and at regional scale, Tikirt  
121 sandstones end with a continuous level of red claystones 8 to 15 meters thick (fig. 2).

## 122 2.2.2 The Tata Group

123 This Group includes, from oldest to youngest, the formations of Igoudine, Amouslek, Issafène  
124 and Tazlaft. The age of the Tata Group varies from the Tomotien (in the lower Cambrian) at its base,  
125 to the Middle Cambrian at its top. (Soulaimani et al., 2013). The Igoudine Formation (50 to 60 meters  
126 thick) is made up of dolostones with microbialite interlayered with clayed siltstones or siltstones. The  
127 Amouslek Formation appears as an alternation of stromatolitic dolostones with heterolitic facies of  
128 clayed siltstones, for a total thickness of 150 to 180 meters. The Issafene Formation is composed by  
129 red claystones and thin beds of sandstones, and it is 30 to 40 m thick (Soulaimani et al., 2013). The  
130 Tazlaft Formation, 90 to 100 meters thick, is composed of sandstones with oblique cross bedding and  
131 mega-ripples marks (Soulaimani et al., 2013).

## 132 3. Methodology and Analytical procedure

133 In order to decipher the complex pattern of geometries and structures, a structural study has  
134 been performed in the field coupled with high density drill control. As a result, well constrained and  
135 high resolution maps and cross-sections have been constructed (fig. 3 to 5).

136 During the field work, 10 samples have been collected from outcrops and 55 samples have  
137 been collected on 9 core drills. 60 polished thin sections were prepared from these samples. They have  
138 been first observed using a Leica DMRX petrographic microscope (transmitted and reflected light  
139 modes). Complementary observations and analyses were carried out using JSM-6400 JEOL Scanning  
140 Electron Microscope (SEM) at ISTO. Polished thin-sections have been first coated by a thin carbon  
141 layer. Acceleration voltage and beam current were 20 kV and 8 nA, respectively. IdFix Software  
142 package was used for data processing. Back-scattered electrons (BSE) imaging mode was used to  
143 reveal the composition variations at microscopic scale, whereas the texture of clayey material was  
144 examined with secondary electrons (SE) imaging mode. The SEM system is coupled to an Energy-  
145 Dispersive X-ray spectrometer (EDS) to make qualitative determinations of the mineral composition.



146 The Managem Group performed analyses on 23 Reverse Circulation drilling's samples  
147 collected at different depths for the following elements: Cu, CuOx, SiO<sub>2</sub>, Al<sub>2</sub>O<sub>3</sub>, Fe<sub>2</sub>O<sub>3</sub>, CaO, MgO,  
148 K<sub>2</sub>O, MnO, TiO<sub>2</sub>, P<sub>2</sub>O<sub>5</sub>, As, B, Ba, Be, Bi, Cd, Co, Cr, Ge, Li, Mo, Nb, Ni, Pb, Sb, Se, Sn, Sr, W, Y,  
149 Zn, Ag and loss on ignition (LOI). "Cu" corresponds to the total copper content and CuOx  
150 corresponds to the non-sulphide copper content. For the major elements analysis, 0.5 g of the sample  
151 is crushed at less than 100µm and it is dissolved by fusion at 500°C during 45 minutes with 2.5 g of  
152 sodium peroxide in a zirconium crucible. The melt mixing is dissolve with 100 ml of hydrochloric  
153 acid (28% HCl) and the solution is analyzed using an ICP-AES ULTIMA 2C using the Jobin Yvon-  
154 HORIBA device. For the other elements, 0.25 g of the sample is dissolved by acid attack (50%HCl  
155 and 50% HNO<sub>3</sub>) microwave-assisted during 45 minutes at 220°C. The solution is then analyzed by  
156 ICP-MS Thermo X'Serie 2.

## 157 **4. Results**

### 158 **4.1. Structural study**

159 The whole sequence undergoes at least one deformation stage. Two types of folds are present.  
160 The first family corresponds to upright folds characterized by sub-horizontal to slightly NW dipping  
161 axes with a NW-SE to NNW-SSE orientation (fig. 3b). They are marked by an axial planar cleavage  
162 particularly developed in the fold hinge zone. Those NW-trending folds are concentrated in a band,  
163 named herebelow "folding band", which displays a width of 150 to 200 meters and is oriented N145°  
164 (fig. 3 and 4). This "folding band" is developed along a N150E-trending vertical fault, folds being  
165 localized in both sides of the fault. The second fold family shows moderately inclined fold's axes to  
166 the NE, oriented NE-SW (fig. 3). The orientation of NE-trending folds is parallel to the direction  
167 (around N30°) of a SE-vergent thrust that outcrops through the entire area (fig. 3). Therefore, at large  
168 scale, the Jbel Laassel area and its ore body appears to be located within a large NE-trending synclinal  
169 developed in the thrust footwall (figure 3). The relations between the two types of folds could not be  
170 observed in the field. In the thrust hanging wall, a similar vertical fault is found northeastward (fig. 3)  
171 with sub-parallel folds and mineralizations along the northwestern prolongation (out of fig. 3).

172 Consequently, we infer that both hanging- and footwall vertical fault segments are part of the same  
173 vertical fault offset by the late thrust. As the fault is vertical, the thrust might have right lateral oblique  
174 slip component of about 300 meters.

175

## 176 **4.2. Jbel Laassel ore bodies**

### 177 **4.2.1. Geometries and orientation**

178 The vertical and lateral extent of ore bodies was delimited by surface cartography and drills.  
179 Part of the outcrops are covered by superficial alteration formations and mining waste. Ore bodies  
180 extend 150 to 250 meters in width (fig. 4), with a maximal longitudinal extension of 400 meters (fig.  
181 3) for an average thickness of around 100 meters (fig. 4 and 6). Mineralization is hosted in Igoudine  
182 and Amouslek Formations and more especially in dolostones and siltstones beds, rarely in lavas or  
183 claystones beds. It is noteworthy that ore bodies are distributed within and along the “folding band”  
184 with an orientation NE-SW i.e., they show the same preferential orientation as that of the folds (fig. 3).  
185 Moreover, on a NE-SW cross section (fig. 4), the ore bodies show thickness variation: in the hinge of  
186 anticlinal the thickness is maximal whereas in the hinge of synclinal the thickness is minimal (fig. 4).  
187 Similarly, the vertical fault strongly controls the ore bodies distribution with a nearly barren  
188 southwestern compartment contrasting with a rich folded northeastern one (fig. 4). On a NW-SE cross  
189 section, the thickness of the ore bodies is constant and does not show significant variation (fig. 5).

### 190 **4.2.2 Mineralogical composition and paragenetic succession**

191 Without distinction between primary and secondary origin, the copper mineralization is  
192 composed of chalcocite, bornite, chalcopyrite, covellite, digenite, malachite, chrysocolla, tenorite,  
193 native copper and cuprite, associated with quartz, dolomite and calcite as gangue mineral. These  
194 gangue minerals in veinlets or voids systematically show, a banding texture. The observed growth  
195 direction indicates a centripetal quartz, dolomite and finally calcite (fig. 6A). This gangue chronology

196 is a good landmark to determine the copper mineral succession. Bornite appears as minute grains (less  
197 than 20  $\mu\text{m}$ ) in the quartz and dolomite ribbons, equally distributed between these two minerals.  
198 Frequently, lamella exsolutions of chalcopyrite are observed in bornite grains. Chalcocite occurs in  
199 ribbon between the bands of dolomite and calcite. Chalcocite grains mostly appear with an anhedral  
200 shape without internal structure. Sometimes this mineral displays a hexagonal cleavage (fig. 6B and  
201 6C), suggesting, in this case, a primary origin at above 103°C (Ramdhor, 1969). This generation of  
202 chalcocite is named CC1. Beside, chalcocite exists in association with covellite, digenite and  
203 chalcopyrite, in replacement around the bornite, in this case chalcocite, covellite and digenite can be  
204 interpreted as cementation assemblage. This chalcocite is named CC2. Malachite replaces chalcocite  
205 and dolomite and may be replaced by chrysocolla. Malachite also replaces cuprite but sometimes the  
206 opposite situation is observed. Veinlet fills only by malachite are been observed, they cut all the other  
207 rock components and structures except chrysocolla.

208 All these relations between minerals allow to discriminate a primary origin represented by:  
209 quartz, bornite, chalcopyrite, dolomite, chalcocite (CC1) and calcite, and a secondary origin  
210 represented by: covellite, digenite, chalcocite (CC2), malachite, chrysocolla, tenorite, native copper  
211 and cuprite (fig. 7). Based on intersections relations between the different mineral phases, several  
212 episodes of fissuring have been observed (fig. 7).

#### 213 **4.2.3 Multiscale observations of the ore texture**

214 At macroscopic scale, on core samples, two textural types of mineralization have been  
215 distinguished. The most frequent is a stockwork with veins/veinlets parallel or oblique to the  
216 stratification plane (fig. 8). Parallel-bedding veins are still connected to cross-bedding veins (fig. 8C).  
217 The second type corresponds to disseminations within the rock ground mass. Locally it is spatially  
218 related to the stockwork (fig. 8D). When it is well develop, veins of the stockwork can show breccia  
219 texture with angular fragments and in situ fragmentation texture without significant rotation of the  
220 fragment that is characteristic of fluid-assisted brecciation (Jébrak, 1997) (fig. 8A). At the microscopic  
221 scale, both types of mineralization appear composed by the same ore and gangue minerals. Textural

222 and chronological relationships being also similar, both mineralization types have the same  
223 paragenetic sequence (fig. 6, 7 and 8). Veins can also locally show a cockade breccia and quartz with  
224 comb texture (fig. 6F and 6G). At this scale, disseminated grains of copper-bearing minerals, down to  
225 50 micrometers in size, are still observable (fig. 6E). Noteworthy, they frequently show a close spatial  
226 relationship with the veinlet of the stockwork (fig. 6E). At the scanning electron microscope scale, the  
227 disseminated mineralization appears as micro-voids or geodes that display the same mineralogical  
228 content and the same paragenetic succession as that observed at higher observation scales (i.e. with  
229 quartz or dolomite at the wallrock and chalcocite at the center) (fig. 9).

#### 230 **4.2.4 Mineralogical distribution at the deposit scale**

231 Using the data collected on 9 core drills and on surface mapping, the Cu-bearing mineral  
232 abundance is plotted in cross-sections (fig. 4 and 5). The mineralogical abundances are displayed in  
233 the form of spider diagram, with, at the top, the secondary Cu-bearing "oxydized" minerals (malachite,  
234 chrysocolla and cuprite) and at the bottom the primary or cementation Cu-bearing minerals  
235 (chalcocite, bornite and chalcopyrite). The mineralogical abundances are evaluated through  
236 microscopic observations of polished thin sections of mineralized cores. The content of each mineral  
237 is evaluated visually using an abundance chart (Dutro et al., 1989). Results are expressed in the  
238 corresponding axis of the spider diagram in a scale of 0 to 100% with steps of 20%.

239 Chalcocite and malachite are the most abundant minerals in the Jbel Laassel deposit (fig. 4 and  
240 5). According to our observations, no obvious zonation appears between primary sulfides and  
241 "oxidized" mineralization.

242

#### 243 **4.3. Principal Component Analysis (PCA) of chemical data**

244 Two multi-element databases were available for PCA: the larger one, does not include Cu  
245 analyses, while the second one includes Cu analyses for a smaller number of samples. PCA analysis  
246 was performed on both sets separately using varimax criteria.

#### 247 4.3.1. Dataset without copper measurements

248 The first results on database without copper measurements (228 analyses) show that two  
249 factors F1 and F2 explain 42.06 % of the total variability (fig. 10A). Three groups of elements  
250 discriminated in the F1-F2 plane represented by the CaO, MgO and MnO cluster (group 1)  
251 discriminates the carbonate matrix, the second SiO<sub>2</sub>, Al<sub>2</sub>O<sub>3</sub>, K<sub>2</sub>O and B clusters represents the clay  
252 sedimentary component (group 2) whereas the last Co, P<sub>2</sub>O<sub>5</sub>, Fe<sub>2</sub>O<sub>3</sub>, TiO<sub>2</sub> and Pb cluster (group 3)  
253 probably marks the lava component (fig. 10B). Thus, referring to the F1 F2 chemical space (fig. 10C),  
254 the analyzed dolostones consists of alternation of siltstones and dolostone layers, with interstratified  
255 lavas in both of them. It appears that the three groups of variables can be interpreted in terms of  
256 lithology: the groups 1, 2 and 3, corresponding respectively to dolostones, siltstones and lava  
257 formations (fig. 10C).

#### 258 4.3.2 Dataset including copper measurements

259 This data set comprises 72 analyses. For the Cu-mineralized data set (Cu % and CuOx %), the  
260 four first factors account for 80% of the total variance. Beyond factor 4 the explained variance  
261 decreases sharply. The plane F1-F2 represents 48.29% of the total variance (28.27% for F1 and 20.01  
262 for F2). The three petrographic groups previously identified in the F1-F2 plane are well discriminated  
263 by the same element clusters (fig. 10D). This representation of the variables suggests that copper (total  
264 or oxidized) is not linked to any of the three types of lithology. Indeed, copper is independent of  
265 sedimentary dolostones and siltstones, and it is anticorrelated with the lavas (fig. 10D). Moreover, an  
266 examination of the F1-F2 plane, suggests that copper could be associated with barium, but the  
267 correlation coefficient between total copper and barium is -0.05 and that of barium with oxidized  
268 copper is 0.03. This is due to the fact that the total copper, oxidized copper and barium are badly  
269 represented in the plane F1 - F2, as shown in the diagram in figure 10D and by the values of the  
270 weighting coefficients between the original variables and factors. For total copper, oxidized copper  
271 and barium, these values are -0.19, -0.23 and -0.16 with respect to F1 and -0.30, -0.38 and -0.38  
272 relative to F2. The factors where copper (total and oxidized) is best represented are F3 and F6. The

273 weighting coefficients between the copper, the oxidized copper and the factors are 0.54 and 0.42 with  
274 respect to F3 and 0.59 and 0.63 relative to F6, respectively. The variables representation in the plane  
275 F3-F6 (17.37% of the total variance, 12.55% for F3 and 4.82% for F6) shows that the variations of the  
276 total copper and of the oxidized copper are not associated with changes in the others variables values  
277 (fig. 10E). Therefore, the PCA highlights the independence of copper (total and oxidized) relative to  
278 the others variables present in the available database, especially that corresponding to lithology.

## 279 **5. Discussion**

280 In the Jbel Laassel copper deposit, at a macroscopic scale, the mineralization is present as a  
281 stockwork and disseminations. The stockwork is composed by veins filled with a primary paragenesis  
282 composed by: quartz, bornite, chalcopyrite, dolomite, chalcocite, calcite and a secondary paragenesis  
283 composed by: covellite, digenite, malachite, chrysocolla, tenorite, cuprite and native copper. The veins  
284 of this stockwork crosscut the stratification plane or are parallel to it. Both vein families always  
285 present the same mineralogy, texture and paragenetic evolution. These observations suggest that, with  
286 respect to the primary sulfide paragenesis, all the stockwork veins are coeval and formed during the  
287 same mineralizing event. SEM observations reveal that disseminations correspond to microcracks and  
288 cavities filled with the same mineralogical content and the same textural characteristics that of  
289 stockwork veins; moreover the disseminated Cu-bearing mineral grains are directly “connected” to the  
290 stockwork veins. Thus, all the primary mineralization, from the macroscopic scale to the scanning  
291 electron microscope scale, is related to the stockwork and deposited during a unique hydrothermal  
292 event of fluid assisted fracturation of the host sedimentary rocks. All these observations favor an  
293 epigenetic origin of the Jbel Laassel mineralization. In addition, the principal component analysis  
294 shows that copper does not have affinities with any of the lithological groups present in the area. This  
295 result is also consistent with an epigenetic origin of the mineralization. The limits of the ore body  
296 correspond to the limits of the “folding band” (fig. 3). In the cross-section perpendicular to the main  
297 extension of the folding band (fig. 4), the ore body is concentrated in the anticline hinges and his  
298 thickness decreases in syncline hinges; whereas in cross section parallel to the main extension of the  
299 folding axis, the ore body is continuous and does not show noticeable thickness variations (fig. 5).

300 Consequently the mineralized stockwork is clearly controlled by hectometric folds, which are, with the  
301 Igoudine and Amouslek Formations, the trap of the mineralization. Available structural and fault  
302 analysis data do not allow us to decipher clearly the control exerted by the vertical faults on NW-  
303 trending mineralized folds. However, the structural pattern associated with the "folding band" suggest  
304 folding developed within the cover above fault involving basement through drap folding and/or  
305 flower structure mechanisms (Sylvester, 1988; Fossen et al., 2013).

306 Soulaimani & Burkhard (2008) describes variscan kink bands with a rough cleavage in the  
307 vicinity of Panafrican structures in the basement of the Bou Azzer El Graara inlier. These authors  
308 interpret these folds in terms of the reactivation of Panafrican structures during the late Paleozoic  
309 compression. In the terminal Neoproterozoic to Cambrian's cover, folds are currently attributed to this  
310 Paleozoic compression, controlled by the movement of inherited basement structures (Leblanc, 1972;  
311 Soulaimani, 1997; Faïk et al, 2002; Soulaimani & Burkhard, 2008). It results in Bou Azzer-El Graara  
312 inlier, metric to decametric folds, have NW-SE trending axes exhibit with a subordinate NE-SW  
313 orientation (Soulaimani & Burkhard, 2008). The folds in the "folding band" of Jbel Laassel display the  
314 same characteristics as the ones given by Soulaimani & Burkhard (2008), for the Variscan folds, i.e.  
315 metric to decametric folds and NW-SE trending axes with a subordinate NE-SW orientation. In such  
316 conditions, the age of the mineralizing event could probably be contemporary to the deformation or  
317 younger. It could be possible that the intersection between the "folding band" and the NE-SW  
318 synclinal took a role in the trap of mineralization formation. This "folding band" is associated with a  
319 major NW-SE fault with a kilometers extension. This fault probably acted as a drain for fluids that  
320 formed the mineralization of the "folding band" in the Jbel Laassel area. Anticlinal hinges of the  
321 "folding band" could be a trap for hydrothermal discharges with a fluid-assisted fracturing focused in  
322 these hinges. The major NW-SE fault could be in direct relation with the basement, as reported by  
323 Soulaimani & Burkhard (2008) for the others Variscan faults in the terminal Neoproterozoic to  
324 Cambrian cover. This fault could thus emphasize a basement influence at the origin of the Cu  
325 mineralization of Jbel Laassel. We propose that Cu mineralization hosted in the terminal  
326 Neoproterozoic to Cambrian cover are linked to Variscan reactivation of inherited basement structures

327 and Variscan faults that drained fluids which precipitated its copper content in the anticlinal hinge of  
328 the Jbel Laassel "folding band".

## 329 **9. Conclusion**

330 The copper mineralization in Jbel Laassel area is epigenetic and is controlled and coeval with  
331 decametric folding, whose axes exhibit a NW-SE trend in the Igoudine and Amouslek Formations.  
332 These folds are concentrated in a 150 to 200 m wide band, probably formed during the Variscan  
333 compression. Consequently the mineralizing event took place during this period or later. The  
334 mineralization appears as a stockwork, displaying the same characteristics (texture and mineral  
335 composition) from the macroscopic scale to the scale of the scanning electron microscope, i.e. it shows  
336 a textural autosimilarity regardless the scale. The proposed interpretations therefore should not be  
337 extended to the others mineralization hosted in the Neoproterozoic to Cambrian's cover of the Bou  
338 Azzer El Graara inlier without any further study. On the other hand, for academic but also applied  
339 purposes, this work highlights the necessity to perform more detailed studies of the Cu-occurrences  
340 hosted in the cover of the Bou Azzer El Graara inlier to reevaluate the factors controlling these  
341 mineralizations.

## 342 **Acknowledgment**

343 This work was supported by the research project "CALAMINE" .Fieldwork has been financed by  
344 Managem. Thanks are due to M. Jébrak and P. Ericksson for their accurate and constructive reviews.  
345 We are also indebted to I. Di Carlo (ISTO), P. Pehnoud (ISTO), N. Pothier (ISTO), J.-G. Badin  
346 (ISTO) and S. Janiec (ISTO) for the sample preparation, the assistance for bibliography, analyses and  
347 data treatment.

## 348 **Bibliography**



- 349 Alvaro J.J., Ezzouhairi H., Vennin E., Ribeiro M.L., Clausen S., Charif A., Ait Ayad N., Moreira  
350 M.E., 2006. The Early-Cambrian Boho volcano of the El Graara massif, Morocco: Petrology,  
351 geodynamic setting and coeval sedimentation. *J. Afr. Earth Sci.* 44, 396-410.
- 352 Benssaou M. et Hamouni N., 1999. Paléoenvironnements et minéralisations de l'Anti-Atlas  
353 occidental marocain au Cambrien précoce. *Chron. Rech. Min.* 536-537, 113-119.
- 354 Bouchta R., Boyer F., Routhier P., Saadi M. et Salem M., 1977. L'aire cuprifère de l'Anti-Atlas  
355 (Maroc); permanence et arêtes riches. *C. R. Acad. Sc. Paris* 284, 503-506.
- 356 Boudda A., Choubert G., Faure-Muret A., 1979. Essai de stratigraphie de la couverture sédimentaire  
357 de l'Anti-Atlas : Adoudounien-Cambrien inférieur. *Notes et Mémoires du Service Géologique du*  
358 *Maroc.* 271, 96 pp.
- 359 Choubert G., 1947. L'accident majeur de l'Anti-Atlas. *Comptes Rendus de l'Académie des Sciences*  
360 224, 1172-1173.
- 361 Choubert G., 1952. Histoire géologique du domaine de l'Anti-Atlas. In: *Géologie du Maroc. Notes et*  
362 *Mémoires du Service Géologique du Maroc* 100, 75-194.
- 363 Compston W., Williams J.L., Kirschvink J.L., Zhang Z., Ma G., 1992. Zircon U-Pb ages for the Early  
364 Cambrian time scale. *Journal of the Geological Society, London* 127, 319-332.
- 365 Ducrot J., Lancelot J.R., 1977. Problème de la limite Précambrien-Cambrien: étude  
366 radiochronologique par la méthode U/Pb sur zircon du volcan du Jbel Boho. *Can. J. Earth Sci.* 14,  
367 1771-1777.
- 368 Dutro, J.T., Dietrich R.V., Foose R.M., 1989. *AGI Data Sheets: or geology in the field,*  
369 *laboratory, and office, ed. American Geological Institute, Virginia, U.S.A*

- 370 Faik K., Belfoul M.A., Bouabdelli M. et Hassenforder B., 2002. Les structures de la couverture  
371 Néoprotérozoïque terminal et Paléozoïque de la région de Tata, Anti-Atlas centre-occidental,  
372 Maroc: déformation polyphasée, ou interactions socle/couverture pendant l'orogénèse  
373 hercynienne? *J. African Earth Sci.* 32, 765-776.
- 374 Fossen H., Teysier C., Whitney D. L., 2013. Transtensional folding. *J. Struct. Geol.* 56, 89-102.
- 375 Jébrak M., 1997. Hydrothermal breccias in vein-type ore deposits: A review of mechanisms,  
376 morphology and size distribution. *Ore Geology Reviews* 12, 111-134.
- 377 Kersit, 1984. Internal report, Managem, 40 pp.
- 378 Landing E., 1998. Cambrian subdivisions and correlations. *Can. J. Earth Sci.* 35, 4.
- 379 Leblanc M., 1972. Sur le style disharmonique des plis hercyniens de la couverture, Anti-Atlas central  
380 (Maroc). *Comptes Rendus de l'Académie des Sciences* 275, 803-806.
- 381 Leblanc M., 1975. Ophiolites précambriennes et gîtes arséniés de Cobalt (Bou-Azzer, Maroc). *Notes  
382 et Mémoires du Service Géologique du Maroc*, 280, 306 pp.
- 383 Leblanc M., 1986. Appareil ignimbritique et minéralisation cuprifère: Alous (Anti-Atlas, Maroc).  
384 *Mineral. Deposita* 21, 129-136.
- 385 Maacha L., Ennaciri A., El Ghorfi M., Baoutoul H., Saquaque A., Soulaïmani A., 2011. The J.  
386 La'sal Oxidized Copper Deposit (El Graara inlier, Central Anti-Atlas), in: Mouttaqi A., Rjimati  
387 E.C., Maacha L., Michard A., Soulaïmani A., Ibouh H. (Eds), *New geological and mining  
388 guidebook of Morocco. Volume 9. Main Mines of Morocco. Service Géologique du Maroc,  
389 Rabat*, pp. 117-121.
- 390 Maloof A.C., Schrag D.P., Crowley J.L., Bowring S.A., 2005. An expanded record of Early Cambrian  
391 carbon cycling from the Anti-Atlas Margin, Morocco. *Can. J. Earth Sci.* 42, 2195-2216.

- 392 Pouit G., 1966. Paléogéographie et répartition des minéralisations stratiformes de cuivre dans l'anti  
393 atlas occidental (Maroc). Chron. Rech. Min 356, 279-289.
- 394 Ramdhor P., 1969. The ore minerals and their intergrowths. Pergamon Press, 117 pp.
- 395 Saquaque A., Admou H., Karson J. A., Hefferan, K. & Reuber I., 1989. Precambrian accretionary  
396 tectonics in the Bou Azzer–El Graara region, Anti-Atlas, Morocco. *Geology* 17, 1107–1110.
- 397 Sylvester A.G., 1988. Strike-slip faults. *Geol. Soc. Am. Bull.* 100, 1666-1703.
- 398 Skacel J., 1993. Gisement cuprifère polygénétique de Tazalagh (Anti-Atlas occidental). *Mine,*  
399 *Géologie & Energie* 54, 127-133.
- 400 Soulaïmani A., Le Corre Cl., Farazdaq R., 1997. Déformation hercynienne et relation  
401 socle/couverture dans le domaine du Bas Drâa (Anti-Atlas occidental, Maroc). *J. Afr. Earth Sci.*,  
402 24, 271-284.
- 403 Soulaïmani A. and Burkhard M. 2008. The Anti-Atlas chain (Morocco): the southern margin of the  
404 Variscan belt along the edge of the West African craton. Geological Society of London, Special  
405 Publications 297, 433-452.
- 406 Soulaïmani A., Egal. E., Razin Ph., Youbi N., Admou H., Blein O., Barbanson L., Gasquet D.,  
407 Bouabdelli M., 2013. Notice explicative de la carte géologique du Maroc au 1/50 000, feuille Al  
408 Glo'a. Notes et Mémoires du Serv. Géol. Maroc 532 bis, 140 pp.
- 409 Soulaïmanie A., Michard A., Ouanaimi H., Baidder L., Raddi Y., Saddiqi O., Rjimai E.C., 2014. Late  
410 Ediacaran-Cambrian structures and their reactivation during the Variscan and Alpine cycles in the  
411 Anti-Atlas (Morocco). *J. Afr. Earth Sci.*, 98, 94-112.

412 Thomas R.J., Fekkak A., Ennih N., Errami E., Loughlin S.C., Gresse P.G., Chevallier L.P., Liégeois  
413 J.-P., 2004. A new lithostratigraphic framework for the Anti-Atlas Orogen, Moocco. *J. Afr. Earth Sci.*  
414 39, 217-226.

415 **Figures:**

416 **Figure 1: A:** Schematic geologic map of the Anti-Atlas with occurrences of copper mineralizations  
417 modified from Bouchta et al. (1977). Inliers abbreviations : If, Ifni; Kr, Kerdous; Ir, Igherm; TA,  
418 Tagragra d' Akka; TT, Tagragra Tata; AM, Agadir Melloul; Ze, Zenaga; Sr, Sirwa; Bz, Bou Azzer-El  
419 Graara; Sg, Saghro; Og, Ougnat. **B:** Geological and structural map of the Bou Azzer-El Graara area  
420 with occurrences of copper mineralizations, modified from Leblanc (1975).

421 **Figure 2 :** Lithostratigraphic column for the Jbel Laassel area modified from Soulimani et al. (2013).

422 **Figure 3: (a)** Geological and structural map of the Jbel Laassel area, modified from Kersit (1984); **(b)**  
423 Stereogram (Wulff stereonet, lower hemisphere) of bedding ( $S_0$ ) and fold axes (n, number of  
424 measures).

425 **Figure 4:** Geological cross-section (section location A-A' in the map) with ore body limits and  
426 mineralogical abundance of the copper mineralization which are represented in a spider diagram.  
427 Results are expressed in the corresponding axis of the spider diagram in a scale of 0 to 100% with  
428 steps of 20%. Abbreviations: Mal, malachite; Ccl, chrysocolla; Cup, cuprite; Dg, digenite; Bn, bornite;  
429 Ccp, chalcopyrite; Cc, chalcocite.

430 **Figure 5:** Geological cross-section (section location B-B' in the map) with ore body limits and  
431 mineralogical abundance of the copper mineralization which are represented in a spider diagram.  
432 Results are expressed in the corresponding axis of the spider diagram in a scale of 0 to 100% with  
433 steps of 20%.. Same abbreviations than fig.5.

434 **Figure 6:** Microphotographs of the Jbel Laassel Cu ore. **A:** Vein showing banding gangue texture  
435 with quartz on wall, next dolomite and calcite at center (TL nic. +). **B:** Chalcocite in ribbon between

436 bands of dolomite and calcite (RL, nic. //). **C:** Chalcocite in vein with hexagonal cleavage (RL, nic. //).  
437 **D:** Quartz and chalcocite veinlet link to a vein forming a stockwork (TL, nic. //). **E.1:** Quartz vein  
438 cutting bedding (S0) of siltstone and silicification of the siltstones bedding (TL, nic.//). **E.2:** Same  
439 photography as E.1 but in RL (nic. //), chalcocite in vein and in dissemination in silicified bedding,  
440 these disseminations were observed at SEM scale (see fig.9). **F:** Quartz, dolomite and chalcocite vein  
441 showing micro-cockade breccia texture (TL, nic. //). **G:** Quartz in vein with comb texture and  
442 malachite veinlets cutting other rock components and structures (TL, nic. +). Abbreviations: Cc1,  
443 primary chalcocite; Dol, dolomite; Mal, Malachite; Qtz, quartz. TL, transmitted light; RL, reflected  
444 light; nic. //, parallel nicols; nic. +, crossed nicols; S0, bedding of rock.

445 **Figure 7:** Paragenetic succession.

446 **Figure 8:** Photographs of core drill samples. **A:** Stockwork with gangue minerals, chalcocite,  
447 chrysocolla and malachite, and a fluid assisted breccia texture. **B:** Chalcocite stockwork. **C:**  
448 Chalcocite stockwork with vein secant and parallel to the dolostone bedding. **D:** Veins of chalcocite  
449 cutting the dolostone bedding and chalcocite in dissemination in dolostone but linking to the vein, these  
450 disseminations were observed at SEM scale (see fig.9). Abbreviations are given in figure 7.

451 **figure 9:** SEM photographs of disseminated copper mineralization (see figures 6E and 7D). **A:** BSE  
452 image of a micro-vein (100  $\mu\text{m}$  width) composed by quartz, dolomite and chalcocite. **B:** BSE image of  
453 a micro-vein (25  $\mu\text{m}$  width) composed by quartz, dolomite and chalcocite.

454 **Figure 10:** Results of PCA analyses of the data base without copper (A, B and C) and of the data base  
455 with copper (D and E). **A:** Eigenvalues and cumulative variance function of factors. **B:** Variables  
456 projection in the F1-F2 plane (data set without copper: 228 analysis). **C:** samples lithology project in  
457 F1-F2 plane (data set without copper: 228 analysis) and Variables projection in the F1-F2 plane  
458 without legends. **D:** Variables projection in the F1-F2 plane (data set including copper: 72 analysis).  
459 **E:** Variables projection in the F3-F6 plane (data set including copper: 72 analysis).

460

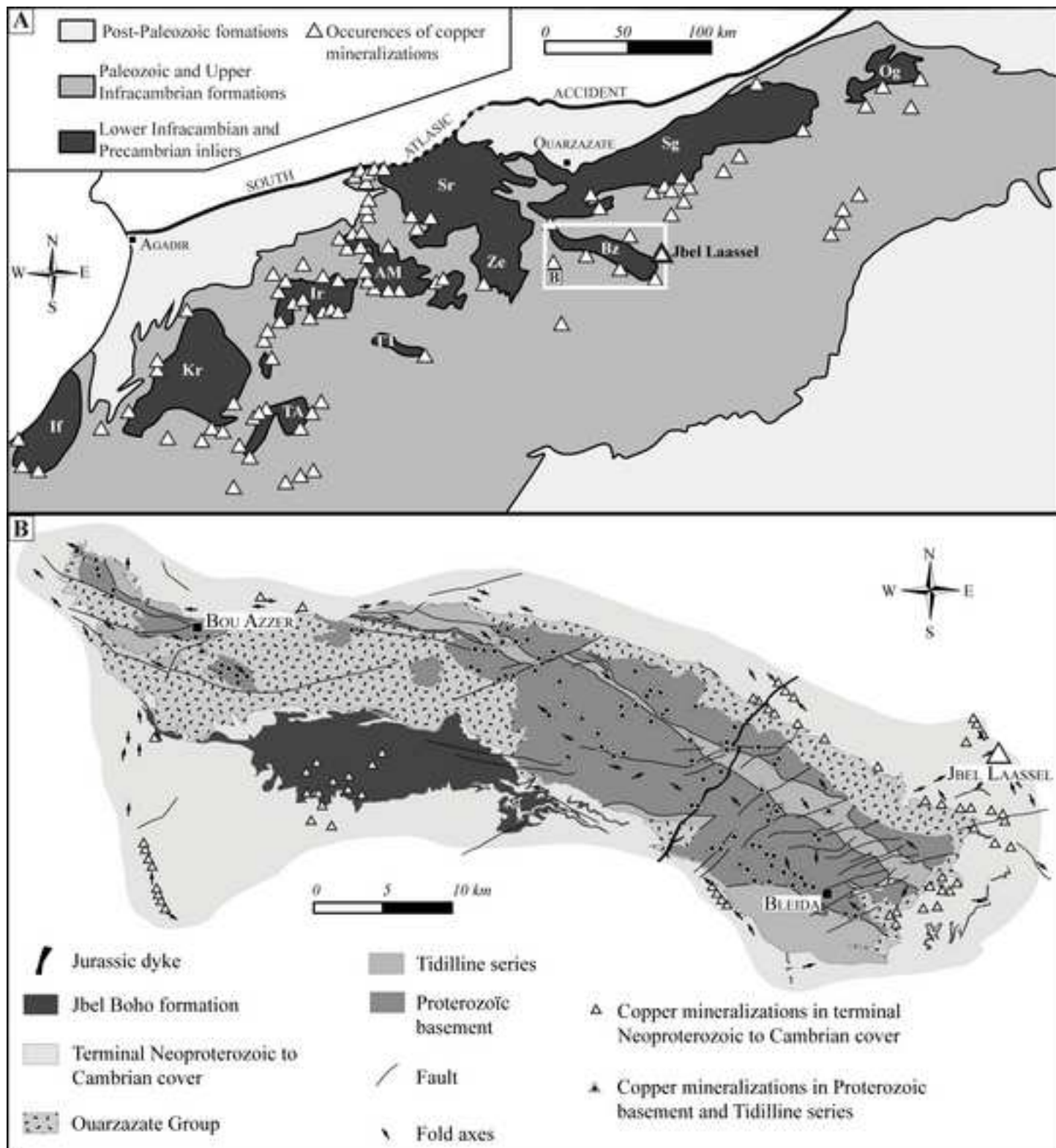


Figure 2

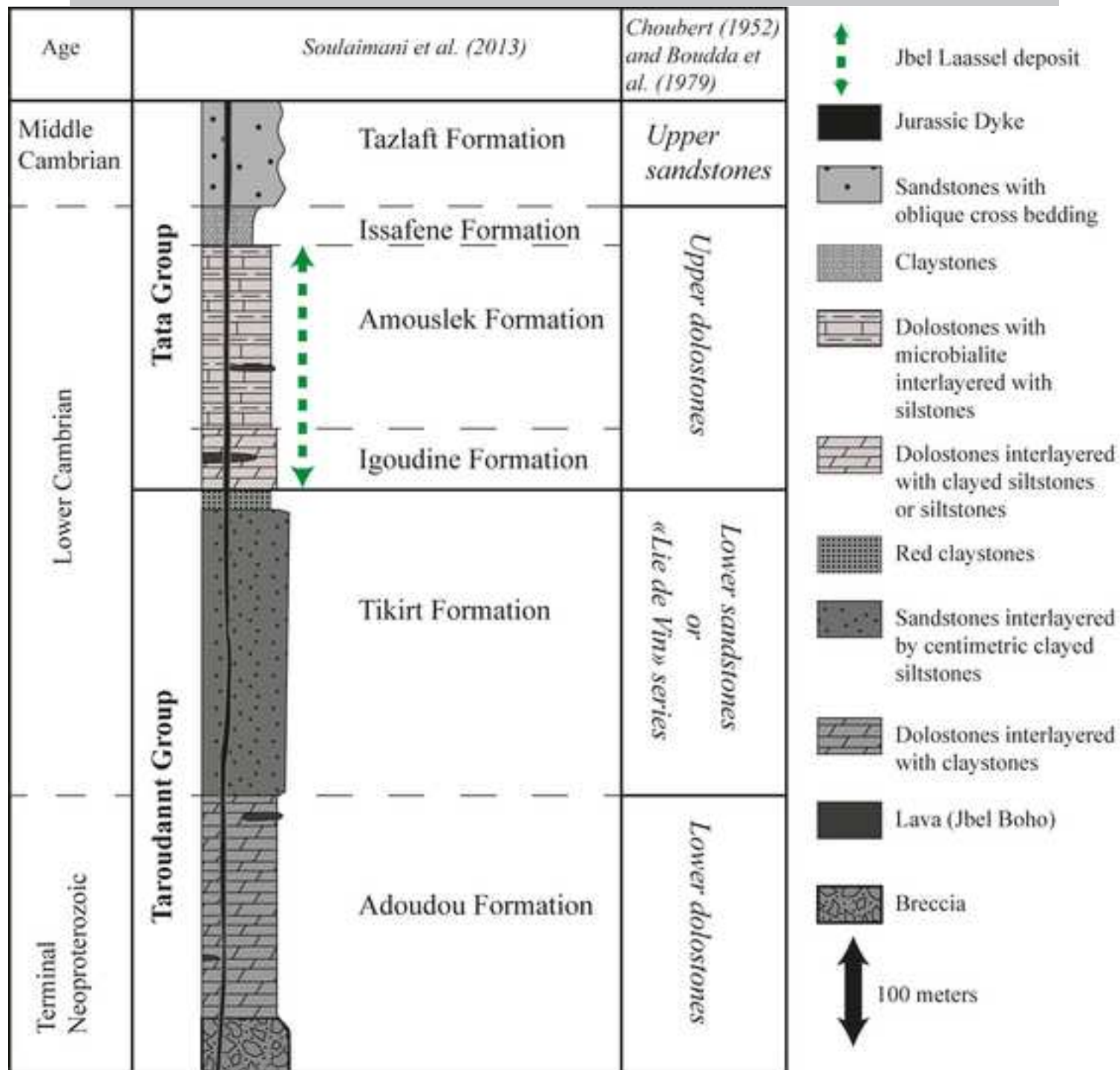


Figure 3

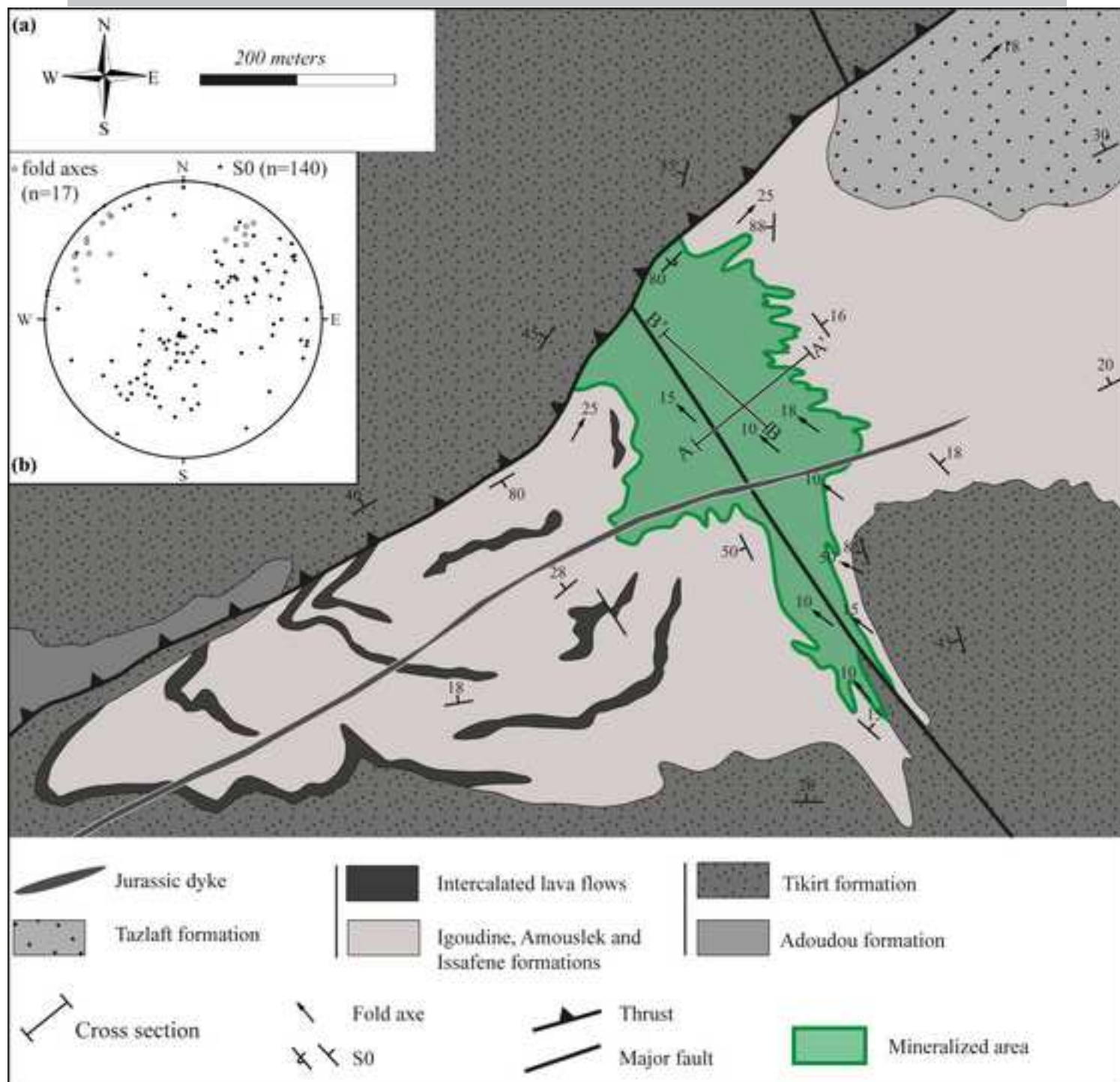




Figure 4

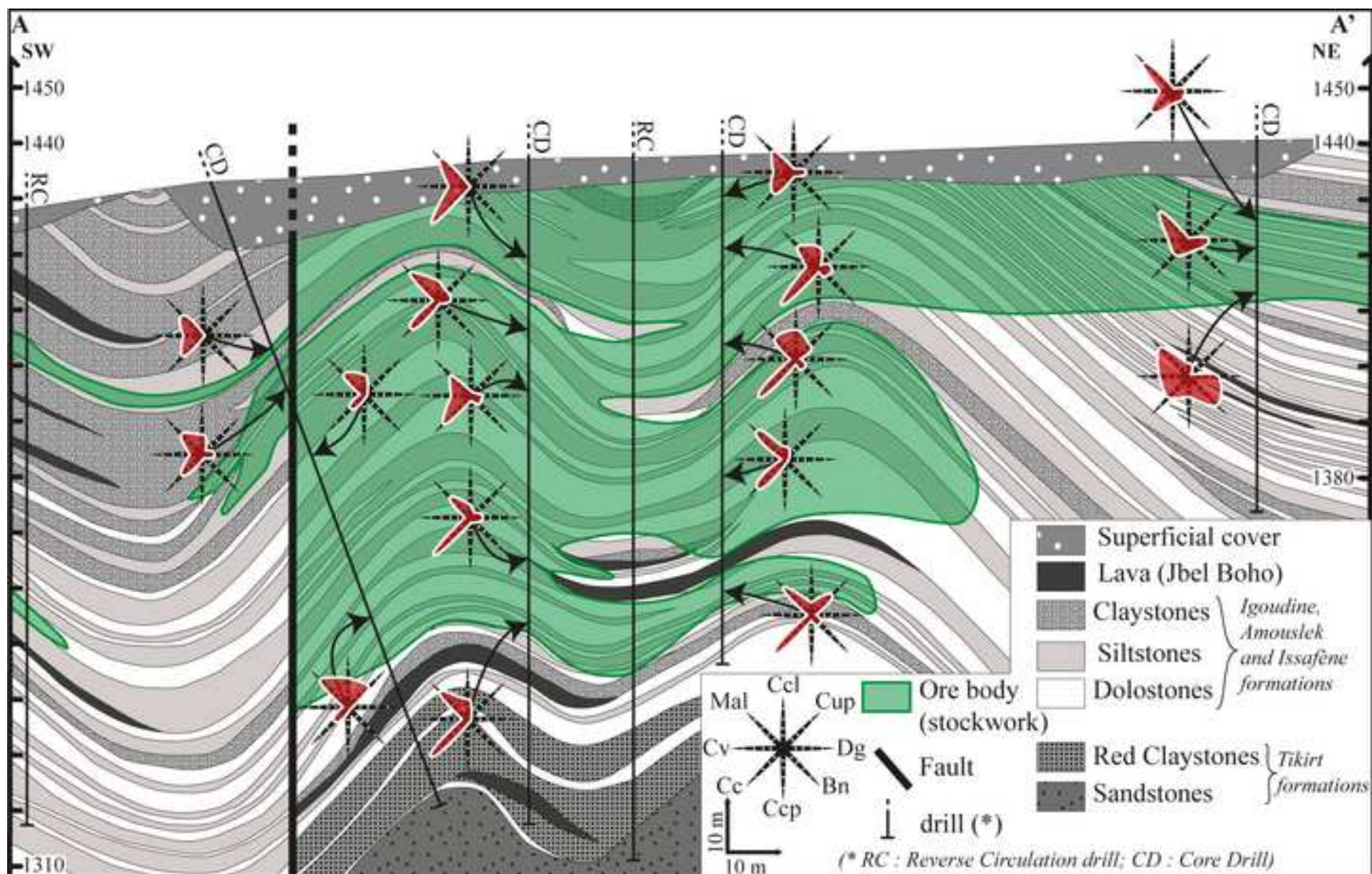
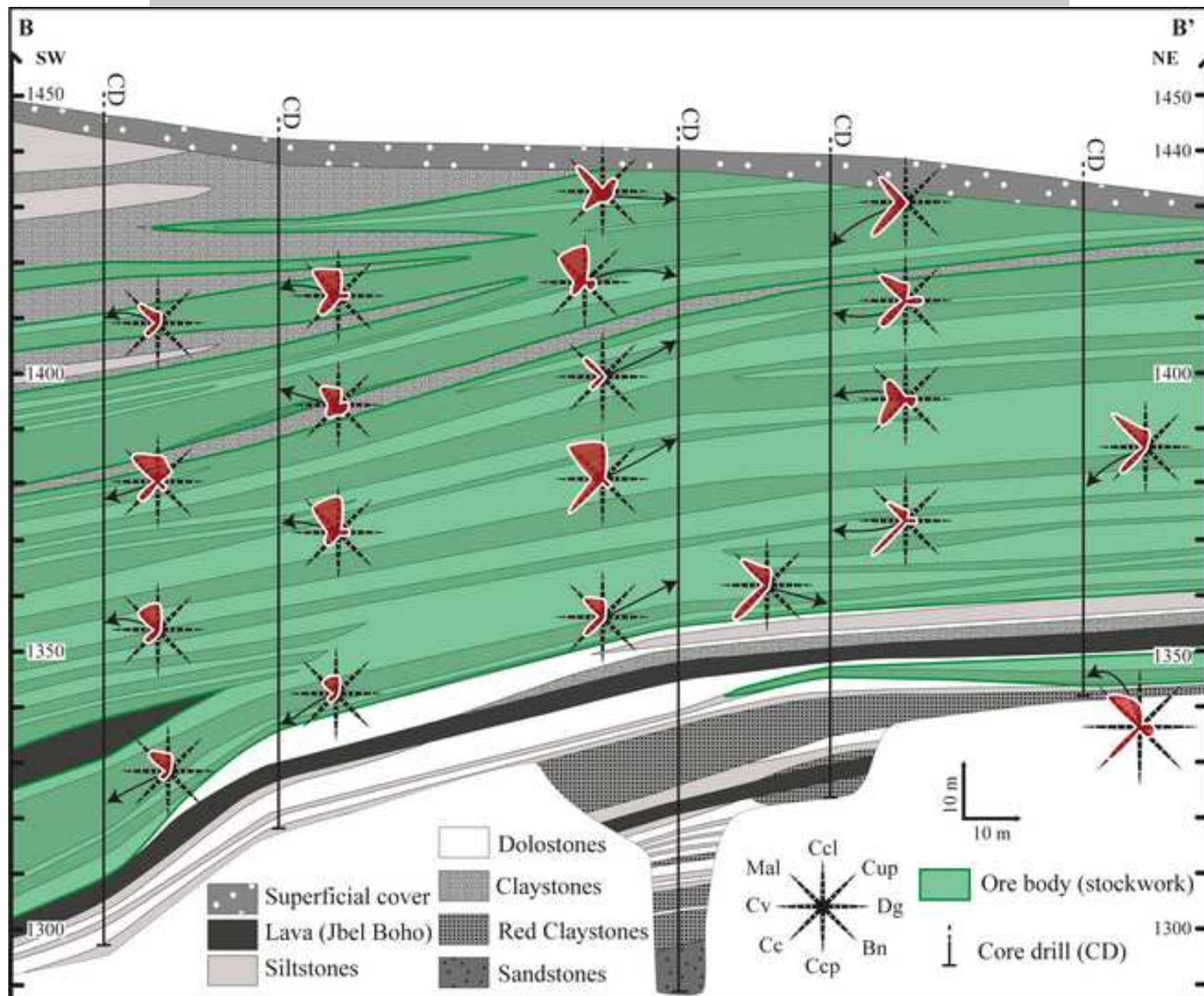
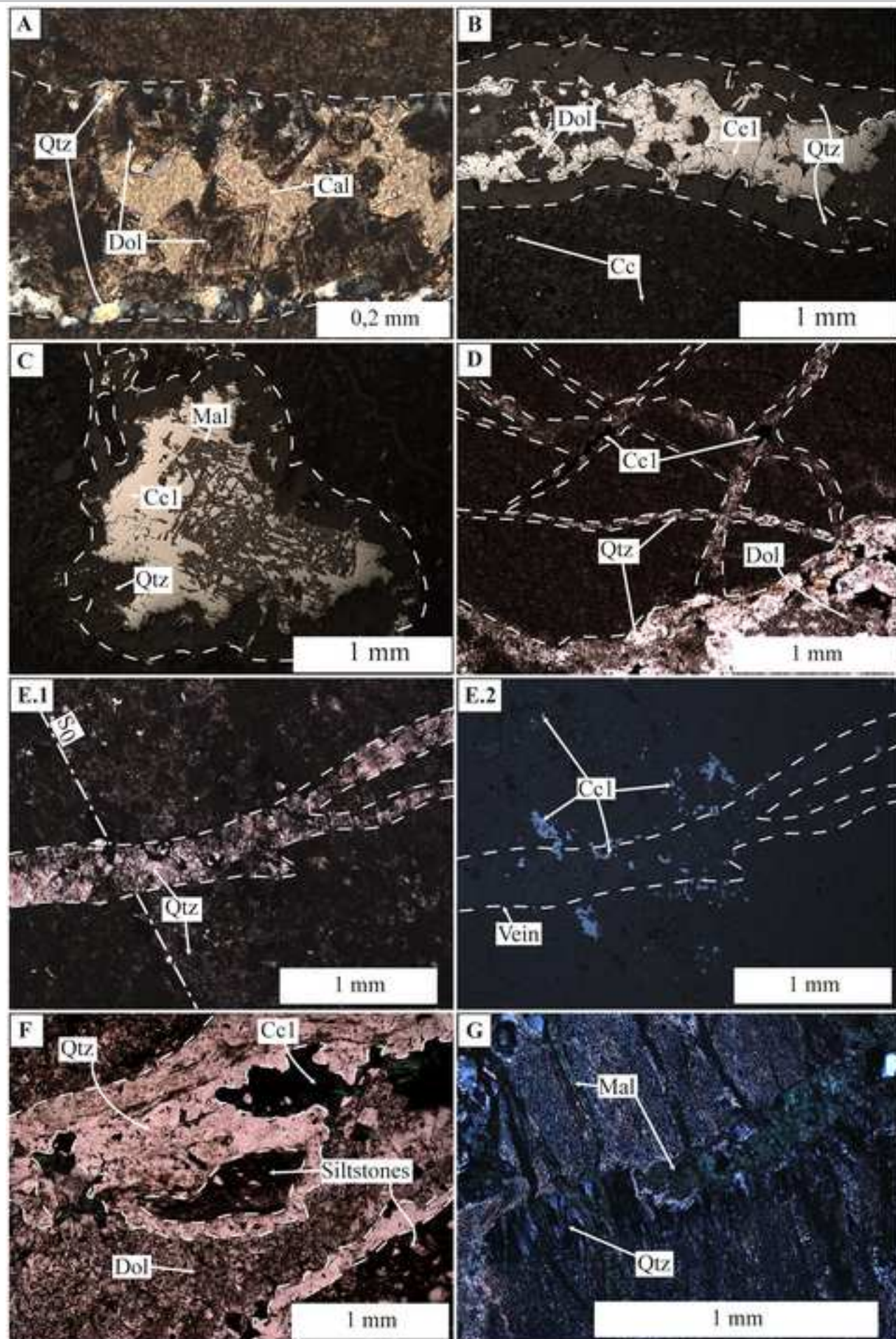
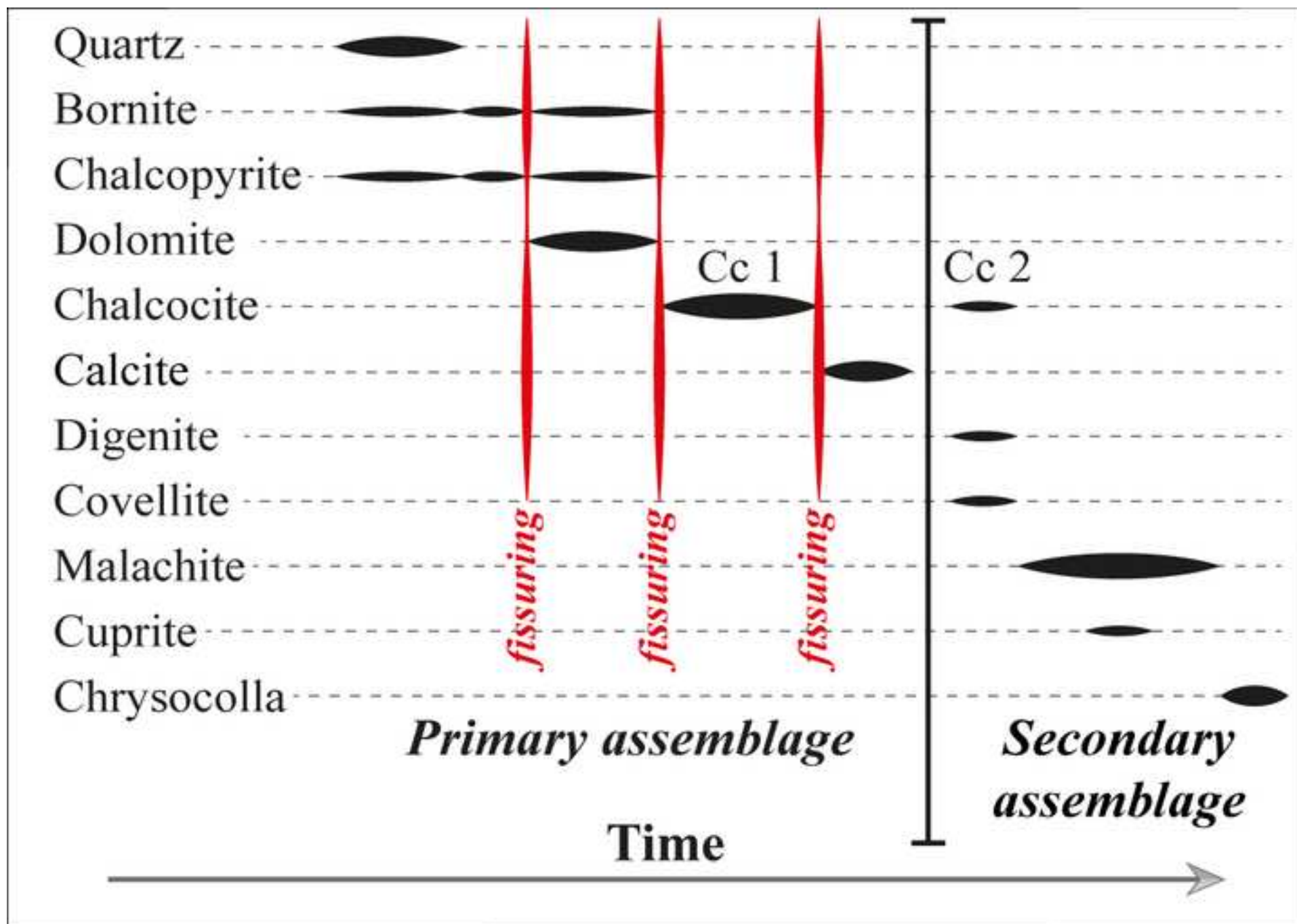
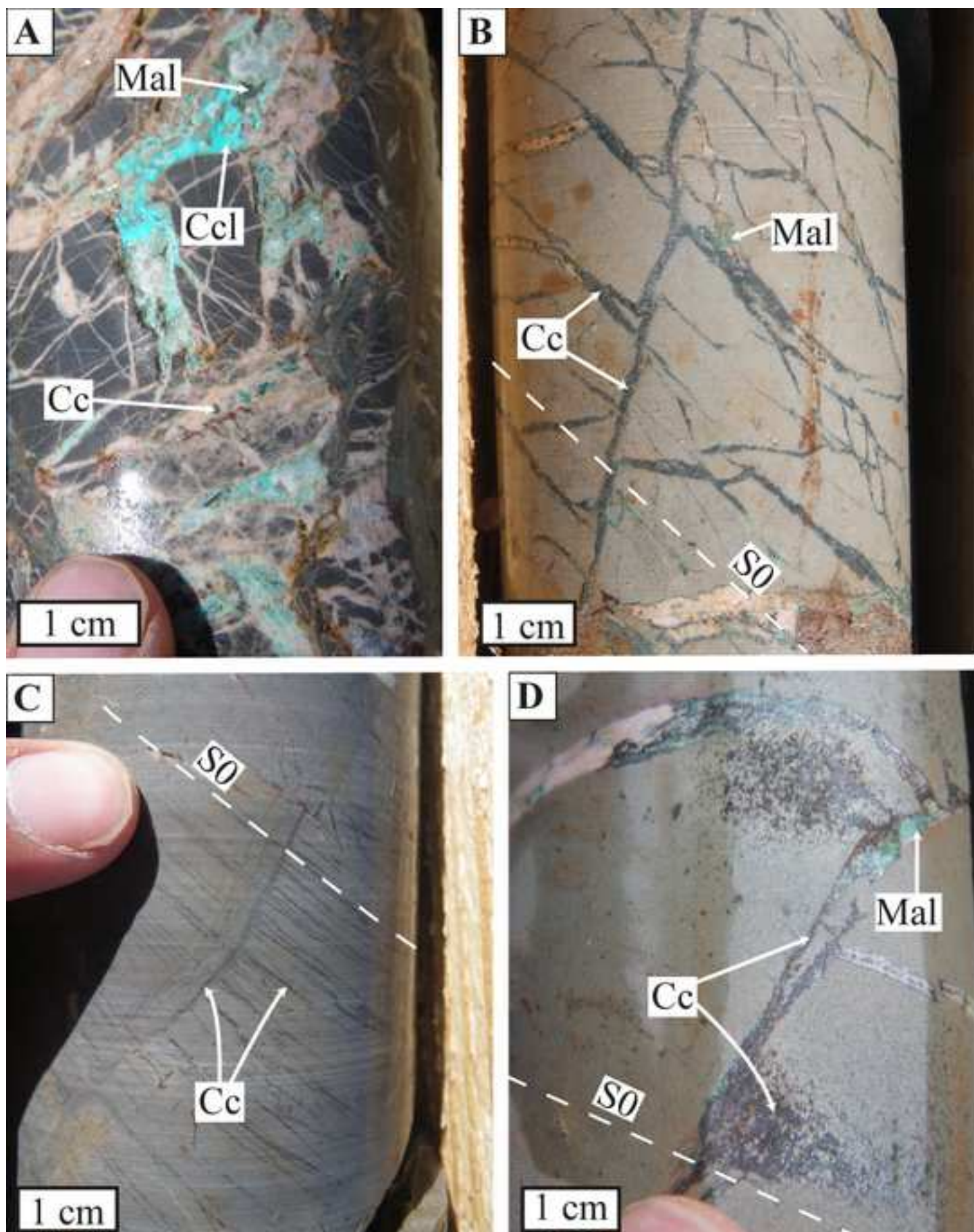


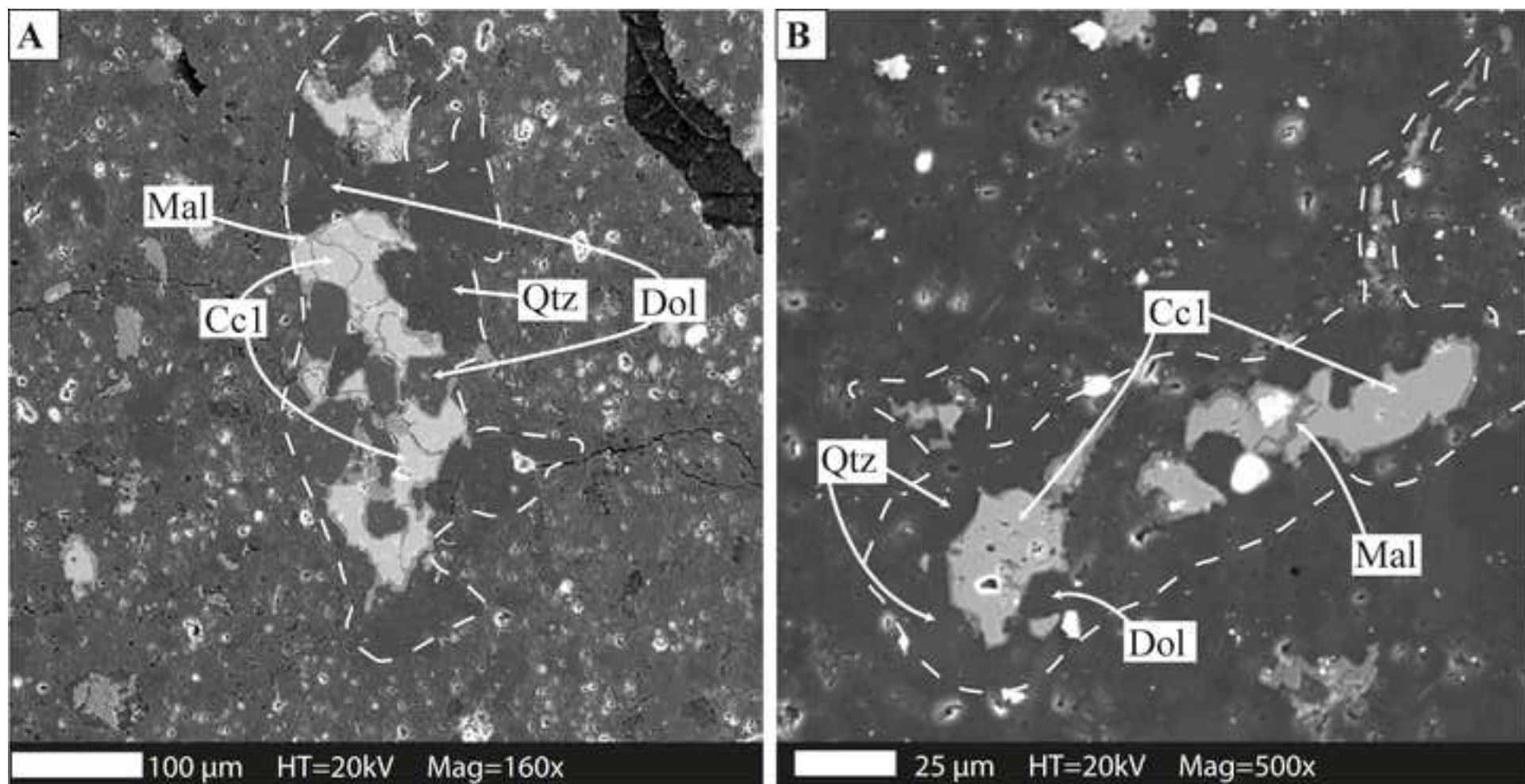
Figure 5

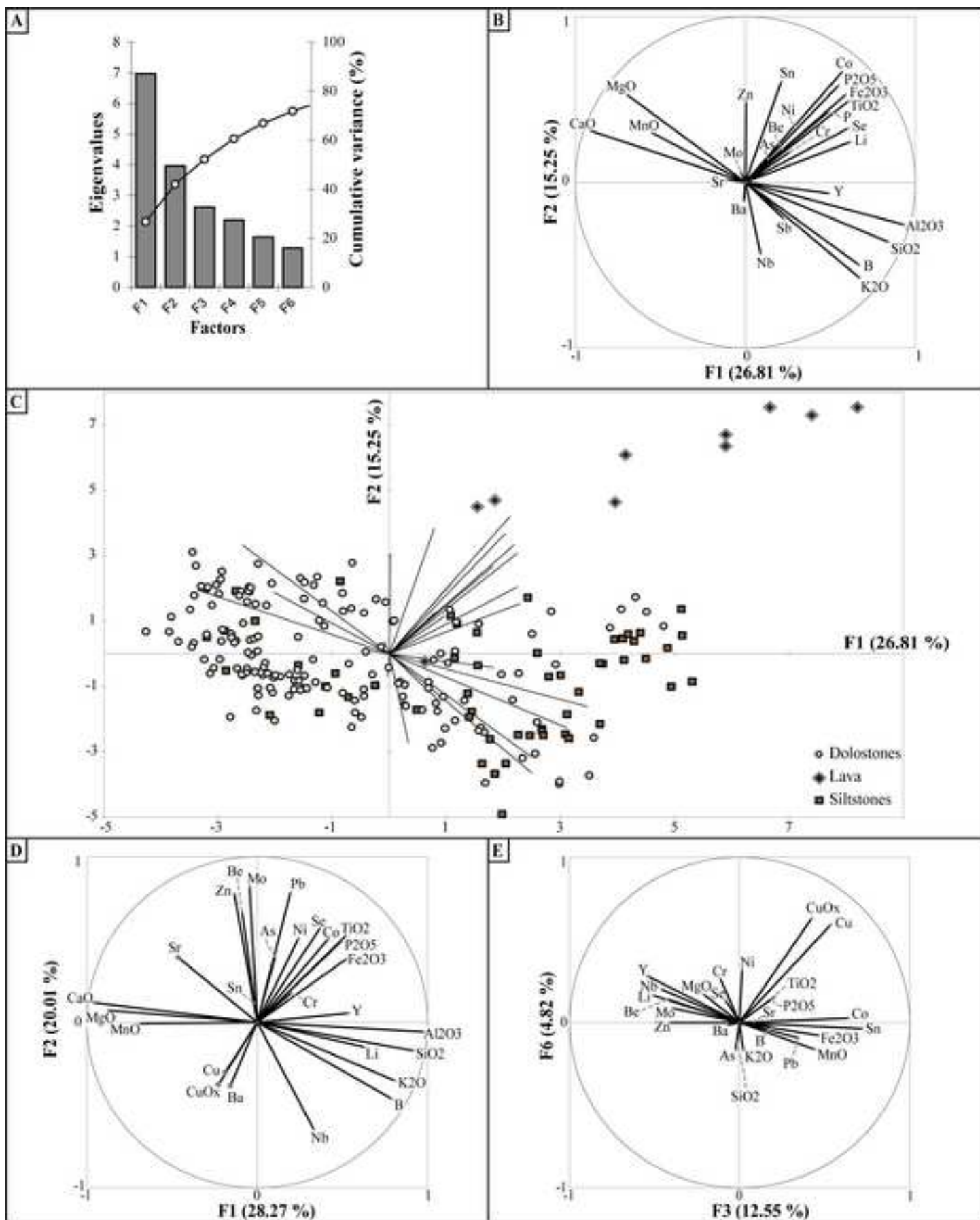












461

462

463 Highlights:

464

- 465 • Copper mineralization occurs in a Variscan folding band in Cambrian cover.
- 466 • The mineralization appears as a stockwork with autosimilar texture.
- 467 • Results from component principal analyses don't show relation with lithology.
- 468 • The Cu-mineralization is epigenetic, controlled by fold axis.

469

ACCEPTED MANUSCRIPT